Progress of Theoretical Physics, Vol. 55, No. 1, January 1976

Potential Energy Surfaces for the Fission of the Actinide Nuclei

Akira IWAMOTO,* Shuhei YAMAJI,** Shota SUEKANE*,*** and Kichinosuke HARADA*

*Japan Atomic Energy Research Institute, Tokai-mura, Naka-gun, Ibaraki
**The Institute of Physical and Chemical Research, Wako-shi, Saitama
***Faculty of Science, Osaka City University, Osaka

(Received November 22, 1974)

Collective potential energy surfaces have been systematically calculated for the symmetric fission of the five isotopes of the elements Th, Pu, Cm, Cf, Fm and No and the eight isotopes of the element U. The calculation is performed on the basis of Strutinsky's prescription in which the liquid drop model of v. Groote and Hilf and the modified two-center harmonic oscillator shell model are used for macroscopic and microscopic parts, respectively. Effects of mass asymmetry at the second saddle point are investigated. The properties of the ground state, the second minimum and the first and second saddle points along the static fission path are discussed in comparison with the results of Möller and Nix. The structure of the potential energy surface is found to come mainly from the shell structure which is strongly related to the distance between the mass centers of the nascent fragments. Special attentions are given to the fragment mass distributions and the constancy of the heavy fragment masses is partially explained on the basis of the properties of the second barrier.

§ 1. Introduction

Since the late 1960's, a renewed interest has been aroused in the structure of the potential energy surface for the fission process. It was motivated mainly by the discoveries of the fission isomer[1] and the related resonant structure of the fission cross section.[2] The calculation based on the liquid drop model was proved not to be able to reproduce these featuers and in 1967 a new method for the calculation of the potential energy—— the macroscopic-microscopic model[3]—— was proposed. Since then, calculations based on this model have been widely made and the fission isomer has been theoretically explained as a shape isomer. It is caused by the shell structure of a largely deformed nucleus and the fact that the shell structure appears at such a large deformation has made a drastic change in our knowledge of the nuclear structure.[4]

The structure of the potential energy surfaces of the heavy nuclei is at present fairly well known.[5]~[8] For the actinide nuclei, a typical feature is that there exists a second minimum and as a result the fission barrier is split into two, the inner barrier and the outer barrier. The calculated heights of these barriers and the second minimum were compared with the experimental data and overall agreement

was obtained. It was also shown that the outer barrier is unstable against the reflection asymmetric deformation and the inner barrier is, for heavy actinide, unstable against the axial asymmetry.[9]

When one uses the macroscopic-microscopic model, one must first specify the basic single-particle potential. Potentials now currently used are the generalized Nilsson potential,[5] the deformed Woods-Saxon potential,[6] the folded Yukawa potential[7] and the two-center harmonic oscillator potential.[8] In this paper, we will report a systematic calculation of the potential energy surfaces of the actinide nuclei based on the two-center harmonic oscillator potential described in Ref. 10). It is one of the simplest potentials that can describe the overall shape change in the nucleus, from the ground state to the separated fragments. Although it has an unphysical wall of infinite height, it can bypass the ambiguity of the treatment of continuum states in the calculation of the shell and pairing correlation corrections. However, this potential cannot describe properly the diamond shape deformation which is necessary for the ground state.

The purpose of the present paper is the following. First, the systematic calculation including the reflection asymmetric deformation has not been done thoroughly yet with this potential, and so the comparison of the potential energy surfaces with other models will be useful. Second, the single-particle level structure at large deformation will be different from other models and the comparison of the single-particle level diagram will be given. In these two respects, the earlier work[8] using the two-center potential seems not to be complete and we think that we can find some new features of this model in our present survey. And third, we will make a detailed analysis of the correlation between the calculated degree of asymmetry at the second saddle and the experimental mass asymmetry of the fragments. It was motivated by the fact that even the folded Yukawa model, which uses a more realistic potential, could not reproduce the experimentally known characteristic of the asymmetric mass yield, that is, the constancy of the mean masses of the heavy fragments. Concerning the question of whether the asymmetric mass yield is determined mainly at the second saddle or not, this analysis will be useful.

As was pointed out earlier, our model cannot describe the ground state deformation precisely and so we will not attach a deep significance to the deformation and energies of the ground states and the absolute values of the heights of the barriers and the second minima. However, our results seem to show clearly the characteristics of the parameterization of the two-center shell model and to reproduce correctly the systematic behavior of the potential energy surfaces.

In § 2, the description of the macroscopic energy and the microscopic energy will be given. The calculations of the shell correction energy and the pairing correlation correction energy have been done following the method of Ref. 11). The details on the shell correction energy were given in Ref. 10). In § 3, the results of the systematic calculations of the collective potential energy surfaces for the fission

of the actinide nuclei will be reported and discussed. In the calculation of the potential energy, the single-particle energy levels of ^{250}Cf are taken as a basis in order to save the computer time. For other nuclei, these levels are shifted proportionally to the ratio of $\hbar\mathring{\omega}_0$ of the relevant nucleus and that of ^{250}Cf. The possibility of an asymmetric mass fragmentation is also examined along the static fission path on the potential energy surface for the symmetric mass fragmentation. In § 4, a brief summary will be given.

§ 2. Macroscopic-microscopic approach

According to Strutinsky's prescription, the collective potential energy of the nucleus is expressed as the sum of the liquid drop energy E_{LDM}, the shell collection energy ΔE_{s} and the pairing correlation correction energy ΔE_{pc},

$$E = E_{\mathrm{LDM}} + \Delta E_{\mathrm{s}} + \Delta E_{\mathrm{pc}} . \tag{1}$$

The first term is the macroscopic part of the potential energy, and the sum of the second and the third terms the microscopic part.

2-1 *Macroscopic part*

For the macroscopic part of the potential energy, the formula of Ref. 12) is adopted. The liquid drop energy E_{LDM} is expressed as the sum of the surface energy E_{surf}, the curvature energy E_{curv} and the Coulomb energy E_{Coul},

$$E_{\mathrm{LDM}} = E_{\mathrm{surf}} + E_{\mathrm{curv}} + E_{\mathrm{Coul}} . \tag{2}$$

Each term is given in the following form,

$$E_{\mathrm{surf}} = \beta_0 A^{2/3}\left[1-\beta_1\left(\frac{N-Z}{A}\right)^2\right](B_{\mathrm{surf}}(s)-1), \tag{3}$$

$$E_{\mathrm{curv}} = \gamma_0 A^{1/3}\left[1-\beta_1\left(\frac{N-Z}{A}\right)^2\right](B_{\mathrm{curv}}(s)-1), \tag{4}$$

$$E_{\mathrm{Coul}} = \frac{3}{5}\frac{e^2}{r_0}\frac{Z^2}{A^{1/3}}(B_{\mathrm{Coul}}(s)-1), \tag{5}$$

where s denotes a set of the shape parameters that characterizes the shape of the nucleus. The quantities $B_{\mathrm{surf}}(s)$, $B_{\mathrm{curv}}(s)$ and $B_{\mathrm{Coul}}(s)$ are the ratios of the surface area, the mean curvature and the Coulomb energy at the shape parameters s to those of the spherical nucleus. The surface of the liquid drop is assumed to be the equipotential surface of the two-center potential whose magnitude is the same as the one at the radius of the spherical nucleus and the volume enclosed by the surface is kept constant. The values of four parameters in Eqs. (3)$\sim$(5) are taken from Ref. 13) as

$$r_0 = 1.123 \text{ fm}, \ \beta_1 = 1.7826, \ \beta_0 = 17.8 \text{ MeV and } \gamma_0 = 6.5 \text{ MeV}; \tag{6}$$

these values were determined by fitting the masses of the ground states and the

fission barriers of the actinide nuclei. However the double humped structure of the potential energy surface is not taken into account in this formula. To check the reliability of this mass formula, the potential energy surface of ^{236}U calculated in this model is compared with that in Ref. 14). It is found that the barrier height calculated in the model of Ref. 12) is about 0.5 MeV lower than that of Ref. 14) but the qualitative features are not changed appreciably. For the calculation of the Coulomb energy, the slice method of Ref. 15) is used.

2-2 *Microscopic part*

The details of the shell correction energy ΔE_s were described in Ref. 10). The order p and the smoothing range γ of the shell correction are taken to be 6 and $1.1\hbar\mathring{\omega}_0$, respectively. The pairing correlation correction energy ΔE_{pc} is calculated following Ref. 11). In this method, ΔE_{pc} is expressed as the difference of the BCS pairing correlation energy E_{pc} calculated from the real single-particle levels and the corresponding quantity $\bar{E}_{pc}$ calculated from single-particle levels with the smoothly averaged distribution using the same strength of the constant pairing interaction as that of the real system.

$$\Delta E_{pc} = E_{pc} - \bar{E}_{pc} . \tag{7}$$

In the case of asymmetric fragmentation, the neutrons and the protons are put into the respective single-particle levels of the asymmetrically deformed potential compactly in order of energy just as in the symmetrical case. The degree of asymmetry is defined as the ratio of the left and right parts of the volume surrounded by the equipotential surface that corresponds to the nuclear surface. Hence the attention should be paid to the fact that this quantity is not related directly to the ratio of the exact numbers of nucleons in the left and right parts of the potential. However, in the following, we use the term "fragment masses" to denote the masses obtained by dividing the mass of the fissioning nucleus according to the ratio of the asymmetry defined above.

As was mentioned in the Introduction, the microscopic part of the potential energy is calculated by taking the single-particle levels of ^{250}Cf as a basis, since it is located near the center of actinide region. In the calculation of the microscopic energy for each nucleus, these levels are shifted proportionally to the ratio of $\hbar\mathring{\omega}_0$ of the nucleus to that of ^{250}Cf. To check the error due to this approximation, we have also calculated the collective potential energies of ^{232}Th, ^{240}Cf, ^{256}Cf and ^{260}No with proper single-particle levels for those nuclei. Check calculations are made at various points, that is, $z_0 = 3$, 6 and 9 fm, for each z_0, δ is set equal to -0.5, 0.0 and 0.5. The results show that the maximum error is 0.35 MeV and for most cases the errors are within 0.1 MeV. From these results, we conclude that with this approximation the potential energy surface can be calculated within the limit of the error ± 0.4 MeV and this error is considered not to cause any serious difficulty in the present analysis. The neck-in parameter ε defined in

Ref. 10) is fixed to be 0.5, as long as it is not specified.

§ 3. The results and discussion

For the five isotopes of Th, Pu, Cm, Cf, Fm and No and the eight isotopes of U, the contour maps of the collective potential energy are plotted as a function of the center separation z_0 and the fragment deformation δ.*) As an example, the potential energy surface for ^{236}U is shown in Fig. 1(a). The contours are labelled by the energy in MeV relative to the spherical liquid drop model energy. The dashed line in the figure represents the static fission path.

The ground state is located at $z_0=0$ fm, $\delta\sim0.2$ and the second minimum at $z_0\sim4.5$ fm, $\delta\sim0.3$. The second minimum in this model has a finite center separation and this means that in the one-center (Nilsson) model, the deformation of the second minimum is described as a linear combination of higher multipole deformations. In fact, the Legendre polynomial expansion of the nuclear surface of the two-center model converges very slowly even when the neck correction is imposed.

In Fig. 1(b), the potential energy surface for ^{236}U is also shown in the

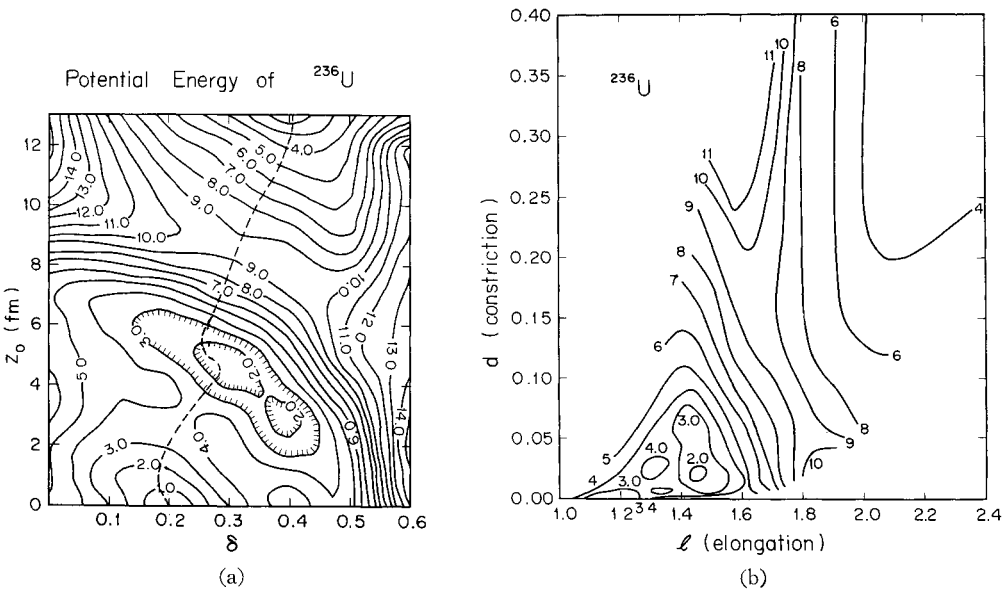

Fig. 1. The collective potential energy surface of ^{236}U. The contours are labelled by the energies in MeV relative to the spherical liquid drop model energy.
(a) A contour map plotted as a function of the center separation z_0 and the fragment deformation δ. The dashed line in the figure represents the static fission path.
(b) A contour map plotted as a function of an elongation parameter l and a constriction parameter d defined in Ref. 16).

*) $\delta=\delta_1=\delta_2$ in a symmetric fragmentation.

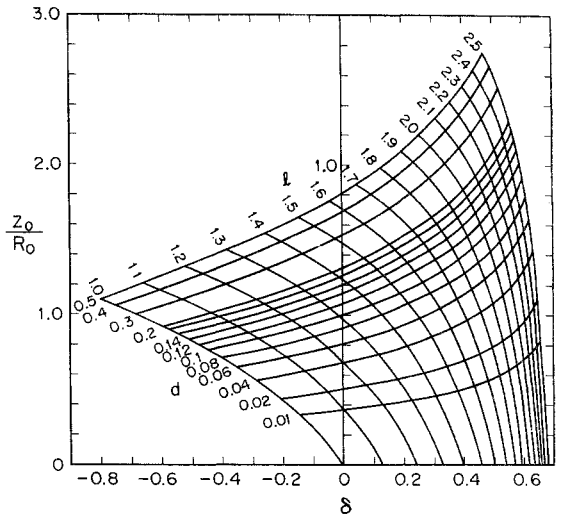

Fig. 2. The relation between the parameters $(z_0/R_0, \delta)$ and (l, d), where l is an elongation parameter and d a constriction parameter as defined in Ref. 16). These two sets of the parameters are connected with the relation

$$l=(z_0/2+c)/R_0, \quad d=1-d_0/a=1-(1-z_0^2/8c^2)^{1/2}.$$

For the definition of a, c and d_0, see Ref. 16).

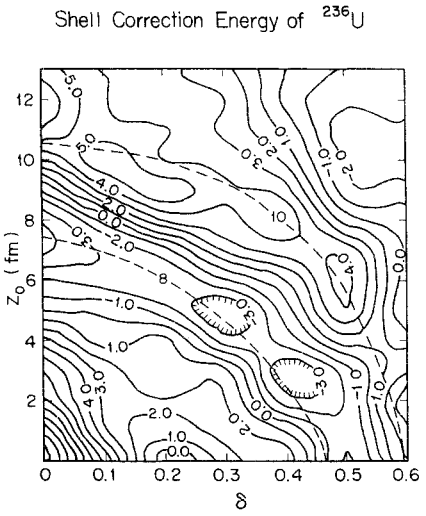

Fig. 3. The shell correction energy surface of ^{236}U as a function of the center separation z_0 and the fragment deformation δ. The contours are labelled by the energies in MeV. The two dashed lines are the contours of constant ρ, where ρ is the distance between the mass centers of the fragments. These are labelled by the constant values in fm.

constriction-elongation representation used in Refs. 16) and 17). The relation between these two sets of parameters is shown in Fig. 2. It can be seen that our calculated result is in accord with that of Ref. 17) and that these two sets of parameters give very different contour maps.

The complicated structure of the energy surface in Fig. 1(a) is mainly caused by the shell correction energy. In Fig. 3 the shell correction energy surface of ^{236}U is shown. From this map the shift of the location of the ground state from the origin ($z_0=0$ fm, $\delta=0$) is seen to be due to the fact that there is a high hill at the spherical shape and is a lake at $z_0=0$ fm, $\delta\sim0.22$. At the position of the second minimum, there is a large valley which extends from $z_0\sim7.5$ fm, $\delta=0$ to $z_0=0$ fm, $\delta\sim0.5$. This latter point has the oscillator frequencies ω_ρ and ω_z connected by the relation $\omega_\rho=2\omega_z$ and is known to be the location that the deformed magic number occur in the spheroidal harmonic oscillator potential. So the single-particle level structure at our second minimum is expected to have a close similarity to the deformed magic structure. The dashed curves drawn in Fig. 3 are those with the condition $\rho=8$ and 10 fm, where ρ is the distance between the mass centers of the nascent fragments. The shell correction energy is seen to be almost costant along the curve. This fact implies that ρ may be a good fission coordinate at an early stage of fission.

In order to understand this fact microscopically, the neutron single-particle levels of ^{236}U are calculated along the dashed curve passing through the second minimum indicated in Fig. 3, and the result is shown in Fig. 4. It is seen that the energy gap at neutron number 144~146 persists from the point $z_0=0$ fm, $\delta=0.47$ to the second minimum.

In Table I, the results of the systematic calculations of the actinide nuclei are collected. In the table, the positions of the ground states, the first saddles, the second minima and the second saddles are shown. Also are shown the ground state energies relative to the spherical liquid drop model energies, heights of the first saddles, the second minima and the second saddles relative to the ground states. Those values may change slightly since in the present work no special consideration is given to the zero-point oscillation. In the last two columns are listed the fragment masses for the most favorable mass division at the second saddle

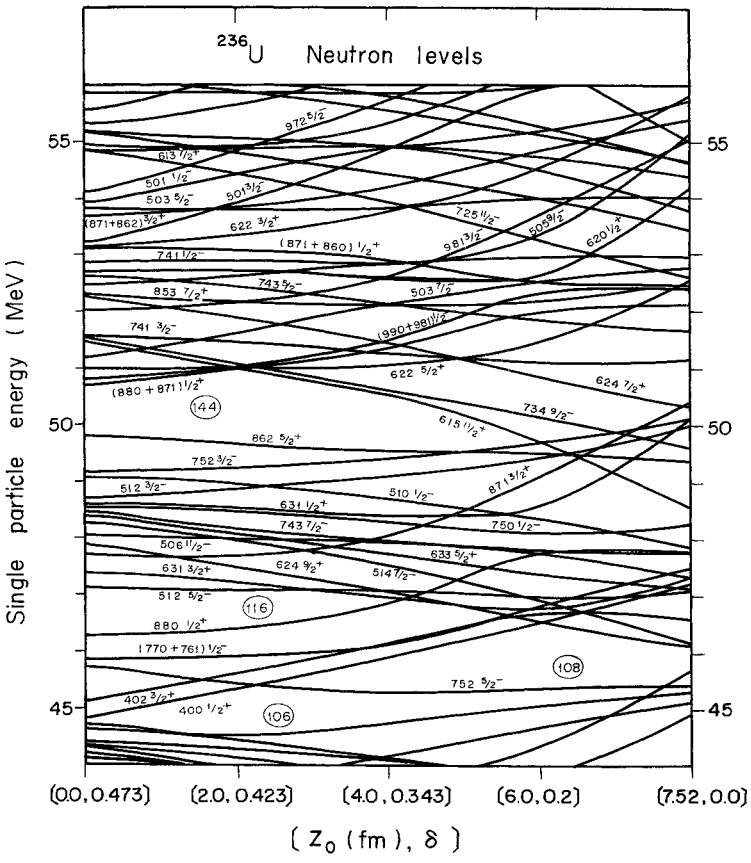

Fig. 4. The neutron single-particle level diagram of ^{236}U as a function of the set (z_0, ρ) along the line with $\rho=8$ fm. The abscissa is labelled by the five sets of the parameters (z_0, δ) all of which lie on the line with $\rho=8$ fm.

Table 1. The calculated locations and energies of the ground state, the first saddle, the second minimum and the second saddle. The ground state energies E_{GS} are measured from the spherical liquid drop model energies and the heights of the first saddle E_{BI}, the second minimum E_{II} and the second saddle E_{BII} are measured from the ground state energies E_{GS}. All energies are in units of MeV and z_0 are in units of fm. The most favorable heavy fragments masses M_H and those of light fragments masses M_L at the second saddle in the symmetric fragmentation are also shown. For the nuclei with asterisks, the contour maps of the collective potential energies differ markedly from those of their lighter isotopes and the locations of the second saddles are very ambiguous. So the mass ratios of these nuclei have little reliability. The locations are determined by the visual measurement from the contour maps of the collective potential energy. The errors due to the procedure are about ± 0.2 fm for the center separation z_0 and about ± 0.02 for the deformation δ.

	ground state			first saddle			second minimum			second saddle				
	z_0	δ	E_{GS}	z_0	δ	E_{BI}	z_0	δ	E_{II}	z_0	δ	E_{BII}	M_H	M_L
$^{232}_{90}Th_{142}$	0.0	0.18	1.3	2.7	0.20	2.3	4.5	0.30	1.0	9.0	0.35	7.3	147	85
$^{236}Th_{146}$	0.0	0.20	0.3	2.7	0.25	4.2	4.5	0.30	1.8	9.0	0.32	7.1	148	88
$^{240}Th_{150}$	0.0	0.20	−0.5	2.5	0.27	5.0	5.0	0.30	3.0	9.0	0.30	8.4	147	93
$^{244}Th_{154}$	0.0	0.20	−0.5	2.5	0.28	5.5	5.6	0.23	3.6	9.8	0.21	9.1	146	98
$^{248}Th_{158}$	0.0	0.19	0.1	2.5	0.29	5.4	5.5	0.56	3.4	13.0	0.11	11.1	129	119*
$^{232}_{92}U_{140}$	0.0	0.19	1.2	3.5	0.23	1.8	4.7	0.29	0.3	8.2	0.35	4.3	147	85
$^{234}U_{142}$	0.0	0.20	0.8	3.5	0.20	2.7	4.5	0.30	0.7	8.5	0.35	5.1	148	86
$^{236}U_{144}$	0.0	0.20	0.2	3.2	0.23	3.2	4.5	0.30	1.3	8.5	0.31	5.3	146	90
$^{238}U_{146}$	0.0	0.20	−0.3	3.5	0.20	4.8	4.5	0.30	1.8	8.8	0.32	6.2	148	90
$^{240}U_{148}$	0.0	0.20	−0.7	2.8	0.25	5.2	4.5	0.30	2.2	8.9	0.30	6.7	147	93
$^{242}U_{150}$	0.0	0.20	−1.0	2.5	0.26	5.8	5.7	0.21	2.7	8.8	0.30	7.3	147	95
$^{246}U_{154}$	0.0	0.20	−1.0	2.4	0.27	6.0	5.9	0.21	3.3	9.0	0.31	7.2	149	97
$^{250}U_{158}$	0.0	0.20	−0.3	2.5	0.28	5.4	5.8	0.26	3.4	11.1	0.08	8.7	130	120*
$^{236}_{94}Pu_{142}$	0.0	0.21	0.1	3.1	0.23	3.4	4.8	0.30	0.5	8.0	0.35	3.4	146	90
$^{240}Pu_{146}$	0.0	0.20	−0.9	2.9	0.24	5.4	4.7	0.30	1.5	8.5	0.30	4.8	145	95
$^{244}Pu_{150}$	0.0	0.20	−1.7	2.5	0.26	6.2	6.0	0.20	2.3	9.0	0.25	6.6	145	99
$^{248}Pu_{154}$	0.0	0.21	−1.6	2.5	0.27	6.1	6.2	0.21	3.0	10.0	0.15	7.8	136	112*
$^{252}Pu_{158}$	0.0	0.21	−0.9	2.5	0.28	5.7	6.0	0.26	3.0	12.0	0.00	6.2	129	123*
$^{238}_{96}Cm_{142}$	0.0	0.20	−0.6	3.0	0.24	3.7	4.8	0.36	0.5	7.6	0.36	2.0	145	93
$^{242}Cm_{146}$	0.0	0.20	−1.7	2.8	0.24	5.6	4.8	0.30	1.4	8.3	0.29	3.8	144	98
$^{246}Cm_{150}$	0.0	0.20	−2.3	2.5	0.26	6.6	6.1	0.21	2.0	8.6	0.28	5.0	145	101
$^{250}Cm_{154}$	0.0	0.20	−2.3	2.4	0.27	6.9	6.3	0.22	2.7	9.6	0.16	6.7	138	112*
$^{254}Cm_{158}$	0.0	0.20	−1.7	2.5	0.27	6.4	6.9	0.19	2.6	9.2	0.04	3.4	127	127*
$^{240}_{98}Cf_{142}$	0.0	0.21	−1.3	3.0	0.24	3.8	5.0	0.30	0.1	7.5	0.35	0.8	144	96
$^{244}Cf_{146}$	0.0	0.21	−2.2	2.7	0.25	5.7	5.0	0.31	0.9	8.3	0.31	2.0	145	99
$^{248}Cf_{150}$	0.0	0.21	−2.9	2.5	0.26	6.7	6.4	0.20	1.6	10.0	0.10	4.3	130	118*
$^{250}Cf_{152}$	0.0	0.20	−2.9	2.5	0.27	6.6	8.2	0.12	1.5	9.4	0.05	3.9	132	118*
$^{252}Cf_{154}$	0.0	0.21	−2.9	2.4	0.27	7.0	9.1	0.00	1.6	10.8	0.00	3.4	130	122*
$^{256}Cf_{158}$	0.0	0.21	−2.9	2.5	0.30	6.8	9.3	0.00	0.6					
$^{242}_{100}Fm_{142}$	0.0	0.21	−1.9	2.8	0.25	4.2	5.3	0.31	−0.4	6.6	0.41	−0.3	141	101
$^{246}Fm_{146}$	0.0	0.21	−2.8	2.6	0.25	5.8	5.1	0.31	0.3	6.5	0.43	1.9	146	100
$^{250}Fm_{150}$	0.0	0.20	−3.4	2.5	0.26	6.8	6.5	0.21	1.1	9.5	0.03	2.6	128	122*
$^{254}Fm_{154}$	0.0	0.20	−3.4	2.5	0.27	7.1	8.1	0.12	1.3	9.5	0.05	1.4	128	126*
$^{258}Fm_{158}$	0.0	0.19	−2.8	2.4	0.27	6.6								
$^{244}_{102}No_{142}$	0.0	0.21	−2.2	2.8	0.25	3.7	5.7	0.33	−1.6	6.4	0.40	−2.2	139	105
$^{248}No_{146}$	0.0	0.20	−3.1	2.7	0.25	5.6	5.4	0.33	−0.4	6.6	0.42	−0.4	144	104
$^{252}No_{150}$	0.0	0.20	−3.7	2.5	0.27	6.6	6.7	0.22	0.2	8.7	0.25	1.0	143	109
$^{256}No_{154}$	0.0	0.20	−3.7	0.5	0.37	6.6	7.3	0.20	0.2	9.8	0.09	0.8	131	125*
$^{260}No_{158}$	0.0	0.20	−3.5	2.5	0.27	7.0								

point on the static fission path for the symmetric fragmentation. These quantities M_H and M_L are obtained with the method in which the potential energies are calculated for five values of the asymmetry and then the interpolation formula of Gauss is used to obtain the most favorable asymmetry. The corresponding barrier heights are denoted as $E_{B\text{II}}$.

In this table we see that the positions of the ground states and the first saddles are fairly constant. The positions of the second minima and the second saddles, however, have a systematic tendency such that as the neutron number increases, the positions shift to larger z_0 and smaller δ. The result of the most favorable mass division will be discussed later.

In Fig. 5 the potential energy curves are shown along the static fission path as a function of z_0/R_0. Arrows show the decrease in the potential energies due to asymmetric fragmentations. One can see from this figure that as the proton number increases, the relative heights of the first and the second saddle change. Note that in the case of ^{236}Pu the height of the second minimum is almost the same as that of the ground state. This figure corresponds to Fig. 5 of Ref. 18). However, it must be noted that the potential energy curve in their figure is shown as a function of the fission coordinate $r=\rho/R_0$.

In Fig. 6 are shown the calculated heights of the second minima and the first and second saddles relative to the calculated ground states as a function of

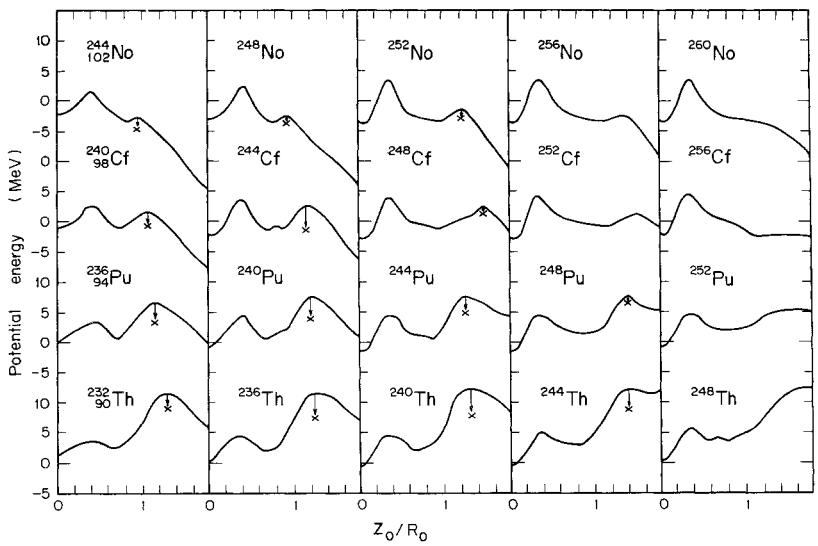

Fig. 5. The collective potential energy curves for various nuclei along their static fission path as a function of the center separation z_0/R_0, where R_0 is the radius of a sperical nucleus. These are determined from the static fission paths on the collective potential energy surfaces and then projected on the z_0-direction. The arrows in the figures indicate the decrease in the collective potential energies due to the asymmetric fragmentation at the second saddle point of the symmetric fragmentation.

the neutron number. The solid lines are our results and the dashed lines are those of the folded Yukawa potential.[7),18)] The experimental data cited in Fig. 10 of Ref. 18) are shown with various marks. As is seen, two theoretical results are in good agreement. This is very surprising, for the single-particle potentials are quite different from each other. From this result, it is surmized that in spite of the apparent difference both potentials give similar level structures near the Fermi level. The agreement with the experimental data is fairly good. To im-

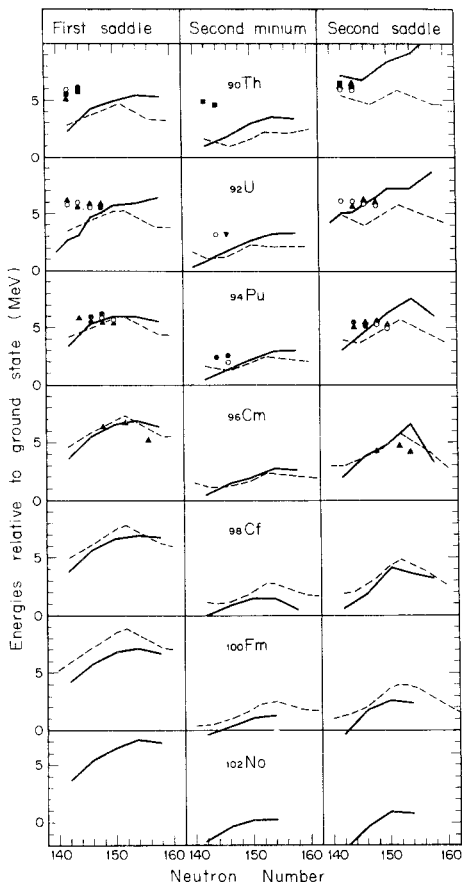

Fig. 6. The heights of the first saddle, the second minimum and the second saddle as a function of the neutron number. The solid lines are the results of the present calculations and the dashed lines are the results of Ref. 18), both of which are measured from the calculated ground states. The various marks represent the experimental data, which are cited from Ref. 18).

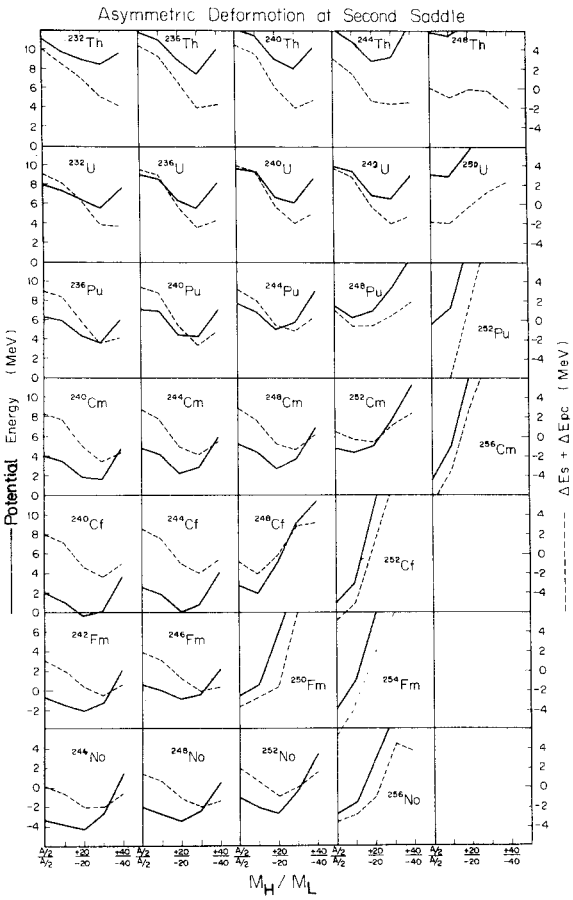

Fig. 7 The collective potential energies and the microscopic correction energies $\Delta E_s + \Delta E_{pc}$ at the second saddle point for the symmetric fragmentation as a function of the mass ratio of the fragments. The abscissa is graduated in units of 20 nucleon difference between two fragments.

prove the theoretical result, many efforts will be needed such as calibration of ground state energy, increase in the number of shape parameters of the potential and inclusion of the dynamics of the fission.

In the above calculations, the degree of freedom of the mass asymmetric fragmentation is included. The first barrier and the second minimum are found to be stable against the asymmetry. However at the second saddle, the inclusion of the asymmetry lowers the barrier height.[5)~8),19)] Effects of the asymmetry are shown in Fig. 7 where the potential energy at the second saddle is plotted as a function of the mass asymmetry. The abscissa is the mass ratio of fragments and left ends of each figure correspond to a symmetric fragmentation. The solid line is the potential energy and the dashed line is the microscopic energy that is a sum of the shell correction and pairing correlation correction energies. From this figure, one can see a tendency that as the neutron number increases in each element, the most favorable mass ratio tends to unity. The lowering of the potential energy due to the asymmetry amounts to zero to four MeV.

The most favorable fragment masses thus obtained are plotted in Fig. 8 together with the experimental data.[20)] In this figure, the masses of the heavy and light fragments are plotted as a function of the mass of the fissioning nucleus. The various lines are our calculated results and the experimental data are shown by various marks. Although there is a small discrepancy in absolute value between theory and experiment, the overall trend of the mass division is well reproduced. In particular, the mass of the heavy fragment is almost constant in our calculation, which is consistent with the experiments.

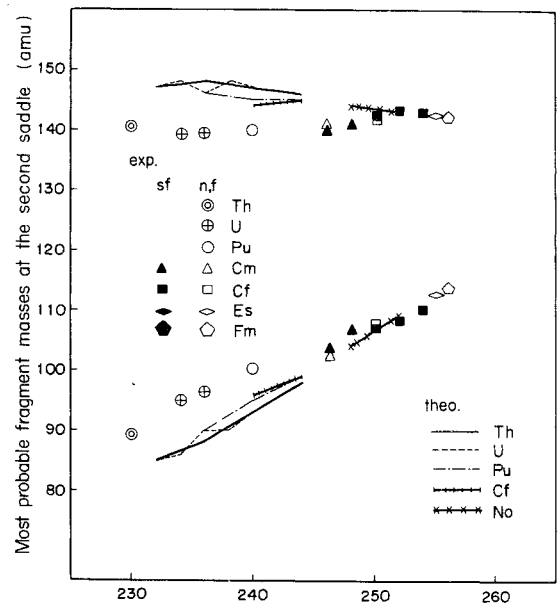

Fig. 8. The most favorable masses calculated at the second saddle. The various lines represent masses of the present calculations. For comparion, the experimental average primary masses of the fragments cited from Ref. 20) are plotted with various marks.

In order to investigate the origin of the mass asymmetry, in Fig. 9 the neutron single-particle level diagram of ^{236}U at the second saddle is shown as a function of the fragment mass ratio. The neutron levels are employed, because the neutrons are more responsible for the asymmetry than the protons.[19)] The symbol n_z in this figure is not the same as the quantum

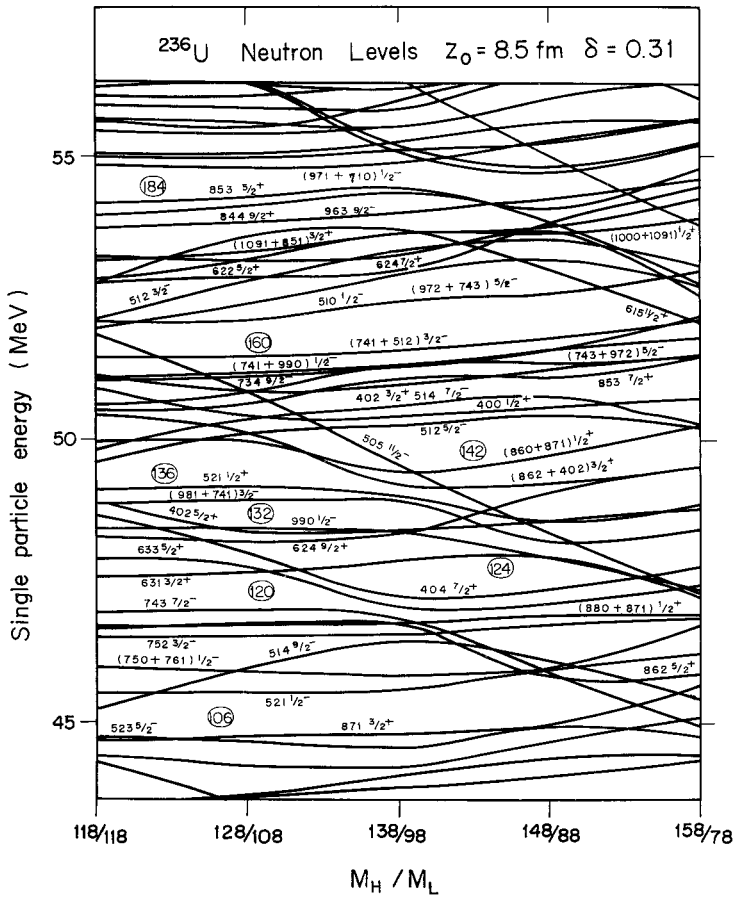

Fig. 9. The neutron single-particle level diagram of ^{236}U calculated at the second saddle point (z_0=8.5 fm and δ=0.31) for the symmetric fragmentation as a function of the mass ratio of the fragments. Each energy level is labelled by the *asymptotic quantum number* $[Nn_z\Lambda]\Omega^\pi$ which is defined here as that of the main component of the wave function at the second saddle point for the symmetric fragmentation. The numbers surrounded by deformed circles are the neutron numbers where the closed shell structure appears.

number n_z of the two-center wave function which is not integer in general. We assign the numbers 0, 1, 2, 3, $\cdots$ to the latter n_z in order of energy and identify these numbers with the former n_z. We should also pay attention to the fact that the main component of the wave function of a level changes as the potential deforms asymmetrically and therefore, the label $[Nn_z\Lambda]\Omega^\pi$ is only meaningful near the symmetric deformation.

In this figure some pairs of levels whose labels are $[N0\Lambda]\Omega$ and $[N+1\,1\,\Lambda]\Omega$, for instance, ([615]11/2$^+$, [505]11/2$^-$), ([512]3/2$^-$, [402]3/2$^+$), etc. can be found near the Fermi level. As was already pointed out in Refs. 21) and 22) these pairs of levels play an important role in directing the fission to an asymmetric

path. The level spacing of these levels is small at symmetric deformation. The reason is that they begin to degenerate according as z_0 becomes large in the case of symmetric fragmentation and as they have small n_z, the degeneracy occurs at an early stage of fission. In addition they are connected with the relation

$$\Delta N=1, \quad \Delta n_z=1, \quad \Delta \Lambda=0, \quad \Delta \Omega=0, \tag{8}$$

so that they have a large matrix element for the octupole deformation. Therefore they repel strongly each other when the potential deforms asymmetrically and then the level spacing between them becomes larger.

The most apparent example of this tendency can be seen in the pair ([615]$11/2^+$, [505]$11/2^-$). There are several such pairs near the Fermi levels of actinide nuclei. These are grouped into two, one consisting of the pairs ([615]$11/2^+$, [505]$11/2^-$), ([512]$3/2^-$, [402]$3/2^+$) and ([510]$1/2^-$, [400]$1/2^+$) and the others ([514]$7/2^-$, [404]$7/2^+$) and ([512]$5/2^-$, [402]$5/2^+$). The former group is slightly above the Fermi level and the latter slightly below at the symmetric deformation. As a result, there occurs a rather large energy gap between neutron numbers 142 and 144 in a rather wide range of asymmetric mass ratio around 144 : 92. This energy gap is most responsible for the formation of the optimum asymmetric fragmentation. As the neutron number increases, the energy of the Fermi level becomes higher than this gap and therefore shell correction energy increases. Therefore the most favorable mass asymmetry becomes smaller with the increase in the mass number of the fissioning nucleus. This effect seems to be most responsible for the fact that the masses of the heavy fragments are fairly constant.

When this single-particle level diagram is compared with that of Fig. 2(b) of Ref. 7) calculated by the folded Yukawa potential at the second saddle, the similarity of the two diagrams can be seen at first glance. However, there is a noticeable difference between the calculated results of the mass asymmetry. According to Ref. 18), the mass asymmetry calculated with the folded Yukawa potential is smaller than the experimental value. On the contrary, our result is larger than the experiment. This could be understood as follows. As the bottom of the folded Yukawa potential is flat in the z-direction unlike the two-center potential used in the present work, the degeneracy of the levels $[N\,0\,\Lambda]\Omega$ and $[N+1\,1\,\Lambda]\Omega$ in Ref. 7) is less than ours at the second saddle for the symmetric fragmentation. Accordingly, the degree of the repulsion of these two levels due to asymmetric deformation is weaker than ours. Hence it will happen that the most favorable mass asymmetry of Ref. 18) is smaller than ours.

In contrast to the neutron case, our proton single-particle level diagram is not so similar to that of Fig. 2(a) of Ref. 7). In Fig. 10, the proton single-particle level diagram of ^{236}U at the second saddle is shown as a function of the fragment mass ratio. From this figure, we can also find some level pairs whose characters are discussed above. These are ([303]$5/2^-$, [413]$5/2^+$], ([301]$3/2^-$, [411]$3/2^+$), ([301]$1/2^-$, [411]$1/2^+$) and ([404]$9/2^+$, [514]$9/2^-$). In this case,

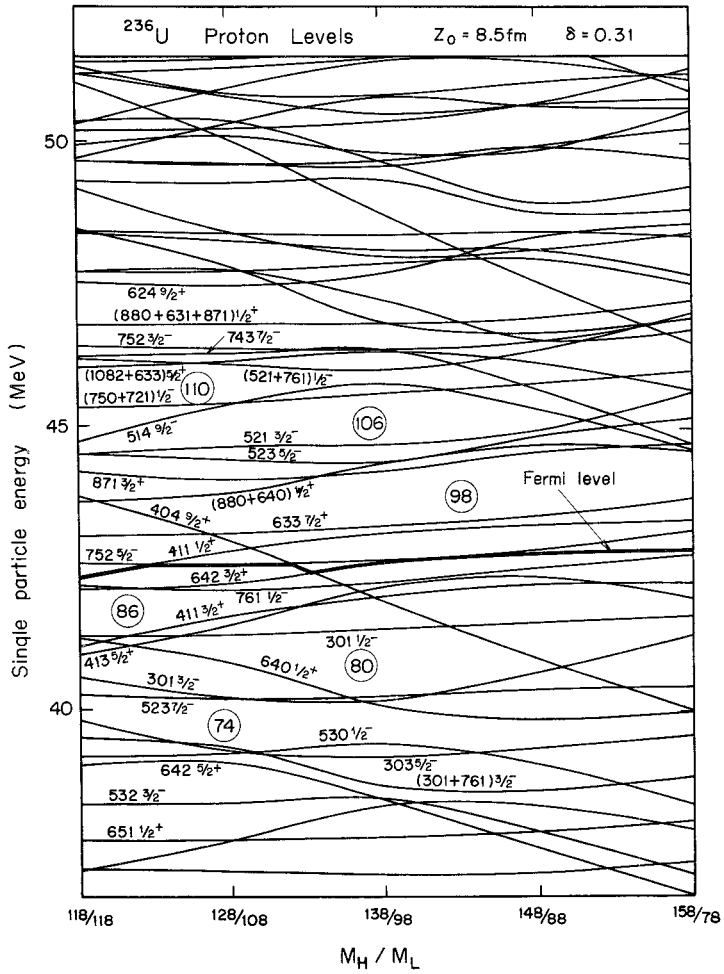

Fig. 10. The proton single-particle level diagram of ^{236}U calculated at the second saddle point (z_0=8.5 fm and δ=0.31) for the symmetric fragmentation as a function of the mass ratio of the fragments. Other notations are as in Fig. 9.

the resultant closed shell structure at proton number 80 seems to be most effective for the occurence of the asymmetric fragmentation. Therefore, in the actinide region we have investigated, the effect of the proton shell on the mass asymmetry is weaker than that of the neutron shell.

The most favorable mass asymmetry was also calculated with the deformed Woods-Saxon potential.[23),24)] In Ref. 23) the mass asymmetry was estimated at the static second saddle, and the estimation in Ref. 24) was made at the "dynamic" outer saddle which is the local maximum of the potential energy surface along the least-action trajectory. So the result of Ref. 24) cannot be compared directly with ours. A comparison between the results of Ref. 23) and of the present work

shows that the former is better than the latter with respect to the peak to peak mass ratio M_H/M_L, while the former is not so good as the latter as to the constancy of heavy fragment masses. Consequently, one can say that the most favorable mass asymmetry is rather sensitive to the details of the single-particle potential.

The neck-in parameter ε is fixed to be 0.5 throughout the present work. In order to obtain the minimum value of the potential energy, the parameter ε must be varied for each set of the parameters z_0, δ and α. However, as it takes a huge computer time to carry out such a variation completely, the ε-dependence of the potential energy of ^{236}U has been examined only at the first saddle, the second minimum and the second saddle. Though it is difficult to mention the general trend of the ε-dependence, the following conclusions are found. In the case of symmetric fragmentation the dependence of the potential energy surface on the parameter ε at these three points is very weak. In particular, the potential energy at the second minimum is nearly constant as the parameter ε changes from 0.3 to 0.7. The values of ε less then 0.5 are favored at the first and the second saddles.

Finally, we must note about the microscopic energies in the region of large two-center deformations. At the later stage of the fission, the fragmentation proceeds more and more and lastly comes to the situation of two separated nuclei. In the present work, we have calculated the shell correction energy by always putting the nucleons into the lowest possible single-particle levels at each deformation, without distinction of the level whether it belongs to light or heavy fragments. Such a calculation will not be correct for a large two-center asymmetric deformation. The pairing interaction adopted in this paper has a constant strength throughout the fission path. The realistic pairing interaction in a fission process, however, may depend on the center separation z_0 and therefore on the fragment state which is occupied by a nucleon pair. These problems deserve to be studied carefully for the detailed discussion of the potential energy surface in the deformation region far behind the second saddle.

§ 4. Summary

A systematic calculation of the collective potential energy surface for the fission of actinide nuclei was performed using the modified two-center shell model developed in Ref. 10). The resultant heights of the first saddle, the second minimum and the second saddle for the fission of these nuclei were fairly in good agreement with the low energy experimental values. It was found that the mass asymmetric deformation has to be included near the second saddle configuration for most of the nuclei studied. The values of the most favorable mass ratio were obtained by the variation method at the second saddle for the symmetric fragmentation and these values were found to be fairly in good agreement with the experimental data. The fact that the masses of the heavy fragment nuclei are

constant was also reproduced systematically and was discussed in connection with the single-particle level diagram.

Numerical calculations were carried out by FACOM 230/75 at the Institute of Physical and Chemical Research and by FACOM 230/60 at Japan Atomic Energy Research Institute.

The authors wish to thank Drs. J. R. Nix and P. Möller for kindly supplying their results prior to publication.

References

1) S. Polikanov, V. A. Druin, V. A. Karnaukhov, V. L. Mikheev, A. A. Pleve, N. K. Skobelev, V. G. Subbotin, G. M. Ter-akop'yan and V. A. Fomichev, Zh. Eksp. i Teor. Fiz. **42** (1962), 1464; Soviet Phys.—JETP **15** (1962), 1016.
2) D. Paya, H. Derrien, A. Fubini, A. Michaudon and P. Ribon, Nuclear Data for Reactors, IAEA, Vienna (1967), Vols. II and III.
3) V. M. Strutinsky, Nucl. Phys. **A95** (1967), 420; **A122** (1968), 1.
4) M. Brack, J. Damgaard, A. S. Jensen, H. C. Pauli, V. M. Strutinsky and C. Y. Wong, Rev. Mod. Phys. **44** (1972), 320.
5) P. Möller, Nucl. Phys. **A192** (1972), 529.
6) H. C. Pauli, Phys. Reports **7C** (1973), 36.
7) P. Möller and J. R. Nix, Nucl. Phys. **A229** (1974), 269.
8) M. G. Mustafa, U. Mosel and H. W. Schmitt, Phys. Rev. **C7** (1973), 1519.
9) S. E. Larsson and G. Leander, 3rd IAEA Symp. Physics and Chemistry of Fission, Rochester 1973 (IAEA, Vienna, 1974), Paper IAEA-SM-174/6.
10) S. Suekane, A. Iwamoto, S. Yamaji and K. Harada, preprint JAERI-memo 5918, unpublished.
11) M. Bolsterli, E. O. Fiset, J. R. Nix and J. L. Norton, Phys. Rev. **C5** (1972), 1050.
J. R. Nix, Ann. Rev. Nucl. Sci. **22** (1972), 65.
12) H. v. Groote and E. Hilf, Nucl. Phys. **A129** (1969), 513.
13) B. L. Andersen, F. Dickman and K. Dietrich, Nucl. Phys. **A159** (1970), 337.
14) W. D. Myers and W. J. Swiatecki, Ark. Fys. **36** (1967), 343.
15) R. Beringer, Phys. Rev. **131** (1963), 1402.
16) U. Mosel and H. W. Schmitt, Nucl. Phys. **A165** (1971), 73.
17) U. Mosel and H. W. Schmitt, Phys. Rev. **C4** (1971), 2185.
18) P. Möller and J. R. Nix, 3rd IAEA Symp. Physics and Chemistry of Fission, Rochester 1973 (IAEA, Vienna, 1974), Paper IAEA-SM-174/202.
19) A. Iwamoto, S. Suekane, S. Yamaji and K. Harada, Prog. Theor. Phys. **51** (1974), 1617.
20) J. P. Unik, J. E. Gindler, L. E. Glendenin, K. F. Flynn, A. Gorski and R. K. Sjoblom, 3rd IAEA Sym. Physics and Chemistry of Fission, Rochester 1973 (IAEA, Vienna, 1974), Paper IAEA-SM-174/209.
21) V. M. Strutinsky, Atomnaya Energiya **1** (1956), 150.
S. A. E. Johansson, Nucl. Phys. **22** (1961), 529.
C. Gustafsson, P. Möller and S. G. Nilsson, Phys. Letters **34B** (1971), 349.
22) B. L. Andersen, Phys. Letters **42B** (1972), 307.
23) H. C. Pauli, T. Ledergerber and M. Brack, Phys. Letters **34B** (1971), 264.
24) T. Ledergerber and H. C. Pauli, Nucl. Phys. **A207** (1973), 1.